



Clay minerals as geo-thermometer: A comparative study based on high spatial resolution analyses of illite and chlorite in Gulf Coast sandstones (Texas, U.S.A.)

Franck Bourdelle, Teddy Parra, Olivier Beyssac, Christian Chopin, Olivier Vidal

► To cite this version:

Franck Bourdelle, Teddy Parra, Olivier Beyssac, Christian Chopin, Olivier Vidal. Clay minerals as geo-thermometer: A comparative study based on high spatial resolution analyses of illite and chlorite in Gulf Coast sandstones (Texas, U.S.A.). *The American Mineralogist*, 2013, 98 (5-6), pp.914-926. 10.2138/am.2013.4238 . hal-02270196

HAL Id: hal-02270196

<https://hal.sorbonne-universite.fr/hal-02270196>

Submitted on 23 Aug 2019

HAL is a multi-disciplinary open access archive for the deposit and dissemination of scientific research documents, whether they are published or not. The documents may come from teaching and research institutions in France or abroad, or from public or private research centers.

L'archive ouverte pluridisciplinaire **HAL**, est destinée au dépôt et à la diffusion de documents scientifiques de niveau recherche, publiés ou non, émanant des établissements d'enseignement et de recherche français ou étrangers, des laboratoires publics ou privés.

Clay minerals as geo-thermometer: A comparative study based on high-spatial-resolution analyses of illite and chlorite in Gulf Coast sandstones (Texas, USA)

Franck Bourdelle^{1,2,3,*}, Teddy Parra², Olivier Beyssac¹, Christian Chopin^{3,†}, and Olivier Vidal⁴

¹ IMPMC, UPMC-CNRS, Campus Jussieu, Case courrier 115, 4 place Jussieu, 75005 Paris, France.

² IFP Energies nouvelles, 1 et 4 avenue de Bois Préau, 92852 Rueil-Malmaison cedex, France.

³ Laboratoire de Géologie, Ecole normale supérieure - CNRS, 24 rue Lhomond, 75231 Paris cedex 5, France.

⁴ CNRS, Université Joseph Fourier Grenoble, ISTerre, BP 53, 1381 rue de la piscine, 38041 Grenoble Cedex, France.

* E-mail address: franck.bourdelle@gmail.com

† E-mail address: christian.chopin@ens.fr

Abstract

Phyllosilicates are among the most important stable minerals within the Earth's crust. Their potential use as geo-thermometer bears great potential for application to the thermal history of rocks within the stability range of layered silicates. A high-resolution analytical technique combining Focused Ion Beam (FIB) milling and Analytical Electron Microscopy (AEM) analysis has been applied to a series of sandstone core samples from the Gulf Coast (Texas,

USA). The nanoscale compositional variations of K-deficient mica and chlorite flakes show that rim compositions are the most likely to approach equilibrium compositions, whereas core compositions may be relict, especially for illite-like phases. These rim analyses were used to test existing empirical or thermodynamically formulated thermo(baro)meters against maximum temperatures, which are perfectly constrained for the selected samples as they were measured *in situ* during drilling (100-230°C and 300-1200 bars). The results show that most of the empirical models overestimate the temperature, while thermodynamic models yields reasonable estimates for diagenetic to anchizonal conditions, especially if the Fe³⁺ content is taken into account. This study clearly shows that phyllosilicates thermometry is reliable when combined with an analytical technique giving access to the fine-scale compositional variations that may represent local equilibration, whereas using micrometric compositional analysis precludes trustworthy application of such thermometers.

Key-words: illite, chlorite, zonation, thermometry, diagenesis, Gulf Coast.

Introduction

Phyllosilicates are widespread minerals in most diagenetic and low-grade metamorphic rocks. For a long time, their compositional variations have attracted interest as potential markers of diagenesis and burial conditions like temperature (*T*), pressure (*P*), rock composition, or fluid availability (e.g. Walshe 1986; Vidal and Parra 2000). These compositional variations reflect the wide possible range of a number of substitutions in phyllosilicates, e.g. di-tri-octahedral, Tschermak or Fe–Mg exchange. Establishing a quantitative link between composition and formation conditions has therefore been a long

pursued goal, with two main approaches: empirical calibrations and thermodynamic modelling.

In the empirical case, Cathelineau and Nieva (1985) and Cathelineau (1988) established a correlation between chlorite tetrahedral Al occupancy (noted ^{IV}Al) and temperature. Their empirical calibrations were subsequently refined by Kranidiotis and McLean (1987), Jowett (1991), Zang and Fyfe (1995) and Xie et al. (1997) to account for the chlorite Mg and Fe contents, which depend primarily on the bulk-rock composition. These empirical thermometers can be easily implemented, but they provide contrasted, sometimes unrealistic, temperature estimates (e.g. De Caritat et al 1993; Essene and Peacor 1995; Vidal et al 1999; Parra et al 2001). More robust thermodynamic solutions have been proposed (Helgeson et al 1978; Helgeson and Aagaard, 1985; Walshe 1986; Aagard and Jahren 1992; Hutcheon 1990; Vidal and Parra 2000; Vidal et al. 2001, 2005, 2006; Parra et al. 2002; Inoue et al. 2009; Dubacq et al. 2010), but they require knowledge of the thermodynamic properties for numerous end-members as well as solid-solution mixing parameters.

The aim of the present study is to compare the results of such thermometers when applied to a low-temperature, diagenetic sample series of well cores for which a direct, *in situ* physical measure of temperature and pressure is available. Indeed, most chlorite and illite thermometers were calibrated either in specific conditions, e.g. a hydrothermal system (Cathelineau and Nieva, 1985), or at relatively high temperatures that were indirectly derived from petrological data, like phase-equilibria, fluid-inclusion or vitrinite-reflectance thermometry.

In addition, several generations of clay minerals showing various compositions generally coexist in the same rock sample, from detrital to authigenic to metamorphic, either as discrete crystals in distinct sites, or as zoned crystals with successive overgrowths on relict cores, which may record part of the clay history. In order to be able to decipher this record in

spite of the small grain sizes and expectedly fine scale of the chemical features, a high spatial analytical resolution is needed. The present study takes advantage of recent developments in combining Focused Ion Beam (FIB) sectioning (e.g. Wirth 2004) and high-resolution transmission electron microscopy (TEM) with coupled energy-dispersive X-ray analysis (EDX). This combination allows both a nanometre-scale resolution of chemical variations and then a detailed investigation of the compositional (and thus crystallization temperature) evolution of phyllosilicates in 2D at the thin-section scale, as it is classically made for metamorphic rocks with electron microprobe analysis (EMPA). The coupled FIB, TEM and EDX techniques were used to explore intracrystalline compositional variations, in an attempt at identifying the compositional domains that may record equilibration at peak temperatures for the key assemblages chlorite + quartz, chlorite + illite and illite + quartz. The relevant compositions were used to test empirical thermometers and the models proposed by Walshe (1986), Vidal et al. (2005) rearranged by Vidal et al. (2006), Inoue et al. (2009) and Dubacq et al. (2010) against the measured T and P in Gulf Coast drill-core samples, considering also the possible effect of the $\text{Fe}^{3+}/\text{Fe}^{2+}$ ratio.

Samples and geological settings

Samples

Thirteen samples from 9 wells were taken from conventional drill cores of the Gulf Coast area (southern Texas, USA), available at the core repository, Bureau of Economic Geology and at University of Texas at Austin (USA). They were selected on the basis of their mineral contents (presence of chlorite, illite-chlorite contacts with a grain size allowing FIB cutting), and to cover the largest range of depth and temperature conditions as possible (cf. Appendix 1).

The selected samples are sandstones and shales of relatively uniform mineralogy, except for the relative amount of clays and/or carbonate cement (cf. Appendix 1). Samples with low or preferably no carbonate content were chosen, to minimize modification of the activity of H₂O. These samples consist mostly of quartz (> 80%), with detrital feldspars, clays (detrital and authigenic) and a minor amount of carbonates (calcite and dolomite), organic matter and pyrite. Clay minerals refer to smectite, I/S, illite, chlorite and kaolinite. The analysed chlorites are devoid of 7 Å phases, as shown by TEM.

Pressure and temperature conditions: thermal history of the Gulf Coast

The last major tectonic event in the Gulf Coast area was the Triassic-Early Jurassic opening of the Gulf of Mexico. Then, the southern part of Texas remained tectonically quiet throughout the Cenozoic Era (Stanley 1986; Posey 1986), with a continuous marine deposition offshore. Thus, the temperature distribution within the sediments remained similar to the classic *T*-depth burial distribution during the Cenozoic, after the thermal anomaly resulting from rifting was dissipated (Nunn 1984). The selected samples are from onshore area, resulting of recent marine regression. At depth, some thermal anomalies exist locally due to advecting fluids moving along the growth faults (Jones 1975; Bodner and Sharp 1988). These anomalies might be due to the presence of salt beds at depth, inducing heterogeneities in thermal conductivity (Bodner 1985), and from a thermal anomaly of the lithosphere (Bodner 1985). However, these thermal anomalies do not affect significantly the eastern area (Frio/Vicksburg fault zone; Pfeiffer 1989). As a consequence, we assume that the present-day *P-T* conditions are the maximum temperatures and maximum pressures reached by each of the samples since its deposition. This assumption was made previously by several equivalent studies (e.g. Hillier and Velde, 1991) and is supported by (i) the regular subsidence and a continuous sediment deposition (Royden et al 1980) during the Cretaceous and the Cenozoic

and (ii) the low erosion rates, from which one can induce that sedimentary deposits are likely to be near their maximum burial depth now (Dutton and Loucks 2010).

Temperature and pressure constraints are bottom hole T and P (noted BHT and BHP, respectively), which were collected from oil and gas well-log headers (purchase by the Bureau of Economic Geology), or from literature recapitulating well-log information (Bodner 1985; Loucks et al 1979; Pfeiffer 1989; McKenna 1997; Bebout et al 1982; Kisters et al 1989; Dodge and Posey 1981; Lynch 1994). The BHT's were corrected by the empirical method of Kehle (1971), which was shown to approach the real temperature within 10 °C (Lynch, 1994). The BHP's were also corrected, taking into account the drilling-mud density and the transition between hydropressure and geopressure regimes as determined by resistivity logs and porosity studies. In summary, the measured temperatures for the selected samples range from 100 to 230°C and the pressures range from 0.3 to 1.2 kbar (cf. Appendix 1). These results are considered as the maximum temperature or pressure undergone by the samples with a tentative uncertainty of ± 20 °C (twice Kehle's method uncertainty) and ± 100 bars (equivalent to ± 700 m in depth).

Analytical procedure

A Scanning Electron Microprobe (SEM) study was carried out on the Hitachi S-2500 instrument at ENS, Paris, operated at 15 kV with a 1.5 nA current intensity, for precisely locating the clay minerals before FIB milling. We then used a FIB 200 FEI of CP2M (University of Aix-Marseille), with a voltage of 30 kV, and a gallium beam. The cutting intensity varied from 5000 to 50 pA and we followed the protocol for FIB-section preparation given by Heaney et al. (2001). Samples were finally analyzed with a TEM-EDX/FIB coupled method and quantitative analyses were deduced and corrected thanks to the *t-O-protocol* (Van

Cappellen and Doukhan 1994; Bourdelle et al. 2012). Twenty-three FIB thin sections were cut from 12 samples, across illite-chlorite contacts near the end of the interface, where recrystallisation is the most likely. The thin foils were cut out with a size of approximately 15 μm by 5 μm and a thickness between 50 and 300 nm. To check for the preservation of the minerals' crystalline structure after FIB-milling, lattice-fringe imaging was then systematically carried out with the TEM.

The FIB sections were analyzed with a TEM-EDX JEOL 2100-F at the Physics and Microanalysis Department of IFPEN (France), using a 200 kV voltage, a counting time of 60 s and a dead time lower than 15%. The current density was maintained at 1.3 pA/cm⁻². The sample tilt angle was 7°. Under these conditions, the spot size was around 1 nm and could be defocused to 50 nm. The EDX analyzer was calibrated on paragonite (Na, Al), pyrophyllite (Al), talc (Mg), muscovite (Fe, Al, K), chlorite (Fe, Al), clintonite (Mg, Ca, Al) and phengite (Mg, Fe, K, Al) and the standardizations were checked against EMP analyses of reference clays (SMB-18; Kohler et al. 2009). Given the high spatial resolution, the analysis points were targeted to reveal within-grain compositional variations (Fig. 1) and, in the case of coexisting chlorite and mica, so as to obtain couples of analyses that may record local equilibrium under changing *P-T* conditions.

The structural formulae were calculated on the basis of 11 and 14 oxygens for illite-like phases and chlorites, respectively, with K, Na and Ca assigned to the interlayer. Several numerical criteria were applied to exclude poor-quality and/or contaminated analyses. For illite-like phases, analyses with either $\text{K} + \text{Na} + \text{Ca} > 1 \text{ apfu}$, $\text{Si} < 3 \text{ apfu}$ or $\text{Si} > 4 \text{ apfu}$ were excluded. For chlorites, analyses with $\text{K}_2\text{O} + \text{Na}_2\text{O} + \text{CaO} > 1 \text{ wt\%}$ (of the 100 wt% total of TEM-EDX analyses) were excluded.

Intracrystalline chemical variations: interpretation and implication for thermobarometry

From the high-spatial resolution dataset yielded by the analytical protocol, analyses were separated into two categories: crystal rim analyses performed at 50 nm of illite-chlorite contacts, and crystal-core analyses (Fig. 1). The comparison of core and rim analyses of illite and chlorite in the selected Gulf Coast samples reveals some systematic trends as a function of measured temperature (i.e. BHT). All the analyses obtained for 2:1 phyllosilicates show K as the dominant interlayer cation, with only traces of Na and Ca. From these observations, Figure 2 presents the K contents of 2:1 phyllosilicates *vs* measured temperature. In the grain cores of each sample, the K content ranges between ~0.5 and 0.8 to 0.98 apfu regardless of the temperature attained (examples of illite rims analyses in Table 1; cf. Appendix 2). In contrast, the maximum K content of the rim analyses increases from ~0.4-0.5 apfu (at ~100 °C) to 0.7-0.9 apfu (at ~230 °C), which reflects the compositional evolution due to illitization (e.g. Perry and Hower 1970; Cathelineau and Nieva 1985; Mathieu and Velde 1989; Lanson and Besson 1992; Battaglia 2004). The rim compositions with maximum K were thus considered to be the compositions closest to equilibrium compositions. Conversely, the K-rich core analyses obtained in the low-*T* samples most likely reflect inherited compositions of detrital material and were not considered further for thermometry. In contrast to the temperature-dependence of the K content, ^{VI}Al (between 1.5 and 2 apfu), Fe + Mg (about 0.6 apfu) contents and XFe (0.5 ± 0.1) show no evolution with temperature for the rim compositions. A variation with *T* of Si content is observable, but not obvious to decipher. The observed trend in K content (Fig. 2) and the possible trend in Si (or ^{IV}Al) content with temperature are accounted for by the combination of the pyrophyllitic (^{IV}Si^{XII}□ = ^{IV}Al^{XII}K) and Tschermak substitutions (^{IV}Si^{VI}(Fe, Mg) = ^{IV}Al^{VI}Al), or any linear combination of them

like ${}^{\text{VI}}\text{Al}^{\text{XII}}\square = {}^{\text{VI}}\text{Fe}^{\text{XII}}\text{K}$ (i.e. octahedral-interlayer exchange), where IV, VI and XII identify tetrahedral, octahedral and interlayer sites respectively, and \square represents octahedral vacancies. According to the observed K contents, we are dealing with illite or K-smectite, simply referred to as illite or K-deficient mica in the following since the thermometers tested consider them collectively.

The tetrahedral Al content (${}^{\text{IV}}\text{Al}$) of core and rim chlorite grains shows a rough increase with T , as expected from earlier studies (Fig. 3). More surprising is the consistently (except at 129 and 191 °C) higher ${}^{\text{IV}}\text{Al}$ maximum value in core than in rim, which is opposite to the trend documented by e.g. Jähren (1991), in zoned authigenic chlorite crystals of the North Sea. This feature suggests that some crystal cores may be of dedrital origin and have retained the high ${}^{\text{IV}}\text{Al}$ content typical for metamorphic chlorites, with their inherent variability. For this reason, only the rim compositions of chlorite were considered for thermometry (examples of chlorite rims analyses are given Table 2 and Appendix 3). In details, these rim compositions of the Gulf Coast chlorites vary with temperature similarly to that reported in previous studies on diagenetic clays (e.g. Velde and Medhioub 1988; Hillier and Velde 1991; Jähren and Aagaard 1989; Jähren 1991; Jähren and Aagaard 1992), with the maximum Al_{total} and ${}^{\text{IV}}\text{Al}$ (mirrored by Si counter-variation) contents both showing an increase with temperature (Fig. 3). The linear evolution of maximum ${}^{\text{IV}}\text{Al}$ with temperature is from ~0.95-1.0 apfu at 100 °C to ~1.38-1.4 apfu at 216 °C (Fig. 3). On the contrary, ${}^{\text{VI}}\text{Al}$ shows no systematic evolution. Another obvious feature is the apparent decrease of octahedral vacancies with increasing temperature. This increase of trioctahedral character with T is a classical feature (e.g. Cathelineau 1988; Inoue et al. 2009), which suggests that, for each measured temperature, those analyses with the highest octahedral occupancy represent the closest approach to the relevant equilibrium composition (as do highest- ${}^{\text{IV}}\text{Al}$ analyses, Table 2). The “equilibrium” vacancy number is then observed to decrease from 0.3 apfu at 102 °C to

0.1 apfu at 232 °C. In contrast, no clear trend of the Fe + Mg content and XFe evolution with temperature is apparent. The compositional variations of chlorite discussed above can be explained by a combination of the Tschermak (${}^{\text{IV}}\text{Si}{}^{\text{VI}}\text{R}^{2+} = {}^{\text{IV}}\text{Al}{}^{\text{VI}}\text{Al}$) and di-trioctahedral substitutions ($2 {}^{\text{VI}}\text{Al}{}^{\text{VI}}\square = 3 {}^{\text{VI}}\text{R}^{2+}$), where \square and R^{2+} represent octahedral vacancies and divalent cations like Fe and Mg, respectively. Their combination in a 2 to 1 ratio would account for the observed variations in ${}^{\text{IV}}\text{Si}$, ${}^{\text{IV}}\text{Al}$ and vacancy, for the near constancy of ${}^{\text{VI}}\text{Al}$, and slight possible increase in R^{2+} . For the two samples at 204 and 232 °C, the ${}^{\text{IV}}\text{Al}$ and ${}^{\text{VI}}\text{Al}$ contents are surprisingly low compared to the general tendency (Fig. 3 and Table 2), and are compensated by large R^{2+} and Si contents. This may be due to a different precursor mineral, a different bulk composition, an Al-poor rock composition or a non-equilibrated mineral chemistry.

From these observations, the chemical variations with T and the differences between crystal core and rim compositions (Fig. 1, 2 and 3) are clearly established at the nanoscale, suggesting a chemical zonation of these phyllosilicates. This zonation can be the result of the dissolution-reprecipitation process occurring along the crystal rims, in accordance to the P - T conditions, in spite of the low- T nature of these phyllosilicates. In addition, the scattering in the dataset observed at each temperature among the crystal-rim compositions (Fig. 2 and 3), for both illite and chlorite, suggests that rim compositions do not all record the last, highest-temperature equilibrium conditions, but that some of them were acquired during earlier stages of equilibration during burial. Indeed, each rim composition refers to a specific part of the P - T history of the crystal, i.e. the different compositions indicate the different steps of crystallisation with T during the burial. As a consequence, only the “extreme” compositions refer to the BHT-BHP. Owing to the difficulty to locate the rim areas that record the last and higher-temperature equilibration, we have considered only the three or four analyses (when it was possible), for each sample, that represent the compositions closest to equilibrium

compositions. This selection of such illite and chlorite rim analyses was used to test the phyllosilicate-based thermobarometers.

Tested thermobarometers

Chlorite thermobarometry

The pioneer chlorite thermometer proposed by Cathelineau and Nieva (1985) and refined by Cathelineau (1988) is an empirical calibration based on a linear increase of ^{IV}Al content with temperature. Several authors (e.g. Shau et al. 1990; De Caritat et al. 1993; Jiang et al. 1994; Essene and Peacor 1995) have criticized the use of this equation as a thermometer, firstly because the chlorite analyses used for the equation calibration were suspected to be contaminated by other mineral phases, and secondly because the ^{IV}Al content of chlorite also depends on the bulk-rock composition. The latter point implies that the thermometer should not been used for other rock composition than the one used for its calibration. In order to take bulk-rock composition effects into account, several tentative corrections were introduced in various empirical equations, mainly based on the $Fe/(Fe+Mg)$ ratio (Kranidiotis and McLean 1987; Jowett 1991; Hillier and Velde 1991; Zang and Fyfe 1995; Xie et al. 1997). All these equations are tested in this study and summarized in Table 3 and Appendix 4.

Alternatively, thermodynamic or semi-thermodynamic models were proposed by Walshe (1986), Vidal et al. (2005, 2006) and Inoue et al. (2009), to estimate P - T formation conditions from chlorite compositions, in most instances considering the chlorite+quartz equilibrium. These models differ by the choice of the end-member components and activity-composition relationships, and by the P - T data used to constrain the activity models (cf. Appendix 4). Moreover, Walshe (1986) and Inoue et al. (2009) neglected the non-ideal contributions and the effect of pressure, whereas Vidal et al. (2005) took them into account. According to the

chlorite structure (Bailey 1988; Holland et al. 1998), two assumptions are also possible for the cationic mixing model: an ordered distribution, which was adopted by Vidal et al. (2005, 2006), or a random mixing, as used by Walshe (1986) and Inoue et al. (2009) (Table 3). In order to test these models, we assumed that $a_{\text{qz}} = 1$ and $a_{\text{H}_2\text{O}} = 1$, which is ensured by the presence of quartz and seems reasonable for low- T chlorite of diagenetic and hydrothermal origin (Inoue et al. 2009), and accounts for the low carbonate content in the rocks. In addition, and contrary to the empirical thermometers, these three thermodynamic models require an Fe^{3+} content estimate to be applied. In this study, $\text{Fe}^{3+}/\Sigma\text{Fe}$ ratios were estimated by the multi-equilibrium approach of Vidal et al. (2006).

K-deficient mica thermobarometry

Battaglia (2004) proposed an empirical illite thermometer directly based on K content with a correction accounting for the Fe-Mg content, which is considered as an indicator of the variation of rock composition. Besides, Parra et al. (2002) proposed and calibrated a thermodynamic model representing the phengite-quartz equilibrium, calculated from activity of chosen end-members and taking into account the non-ideal part of activity coefficients. Dubacq et al. (2010) extended this model to smectite, illite, interlayered smectite-illite and mica by considering the T -hydration relationship, the pressure and the rock composition, and using multi-equilibrium thermobarometry. This model was the first attempt to provide a unique set of 2:1 phyllosilicates thermodynamic properties in a solid-solution model relevant from diagenetic to metamorphic conditions. The model involves an assumed ordered cationic distribution and nine end-members (one of which has several levels of hydration), in order to cover the whole compositional space of 2:1 phyllosilicates (cf. Appendices 1 and 3). The Dubacq et al. (2010) model also considers the non-ideality of cationic exchanges and, on the basis of three independent equilibria and their hydrated equivalent for any smectite, illite or

mica + quartz + water equilibrium, yields a pressure–temperature relation simultaneously with the hydration state (Table 3).

Illite-chlorite assemblages

With the high-spatial-resolution analytical protocol used in this study, we can target pairing of illite and chlorite analyses supposed to represent local equilibria. The relevant heterogeneous equilibrium was envisaged by Walshe (1986) as a thermometer, considering a chlorite + mica + quartz + K-feldspar + water assemblage. The author chose to represent the mica phase with a muscovite structure and a random-mixing cation distribution and ideal activities (cf. Appendix 4). This equilibrium was also used to justify the combination of Vidal et al. (2005, 2006) and Dubacq et al. (2010) models as a multi-equilibrium approach. In this case, the non-ideal ordered models for illite-micas (Dubacq et al. 2010) and chlorites (Vidal et al. 2005, 2006) can be used simultaneously to deduce T and P , assuming the achievement of local equilibrium between chlorites and illites. This is what has been tested and applied in this study to a series of Gulf Coast samples and summarized in Table 3.

P - T estimates from Gulf Coast phyllosilicates

Estimation of $\text{Fe}^{3+}/\Sigma\text{Fe}$ used to test thermobarometers

The chlorite thermodynamic thermobarometers need an estimation of $\text{Fe}^{3+}/\Sigma\text{Fe}$ ratios to be correctly applied. However, measuring the Fe^{3+} content at the nanoscale is challenging, even with the recent methods. For instance, the scanning transmission X-ray microscopy (STXM) and X-ray absorption near edge-structure (XANES) study of Bourdelle (2011, *PhD*) on Gulf Coast chlorites remains only qualitative. In order to circumvent the Fe^{3+} issue, Vidal et al. (2005) and Vidal et al. (2006) proposed a numerical method to estimate a minimum

$X\text{Fe}^{3+} = \text{Fe}^{3+}/\Sigma\text{Fe}$ based on the achievement of convergence of 4 reactions (chlorite+quartz
 and internal chlorite equilibria) at a given pressure, and a maximum $X\text{Fe}^{3+}$ when the
 equilibrium convergence is lost. Vidal et al. (2006) have shown on millimetre-size chlorites
 that the minimum Fe^{3+} content calculated in this way was compatible with XANES
 measurements and can be used as an approximation of the actual Fe^{3+} content. Moreover, the
 difference between estimates of the minimum and maximum $X\text{Fe}^{3+}$ ratios is small in the low-
T contexts. Therefore, we used the multi-equilibrium method proposed by Vidal et al. (2005,
 2006) to estimate the $\text{Fe}^{3+}/\Sigma\text{Fe}$ ratio in Gulf Coast chlorites and used the results as input
 values in Vidal et al. (2005, 2006), Inoue et al. (2009) and Walshe (1986) models (where Fe^{3+}
 replaces $^{\text{VI}}\text{Al}$). This estimated minimum $\text{Fe}^{3+}/\Sigma\text{Fe}$ was found to range between 0.1 and 0.45,
 which seems realistic for low-*T* chlorites (e.g. Inoue et al. 2009) and in agreement with
 literature data and our STXM-XANES qualitative study (Bourdelle 2011, *PhD*). We assumed
 that the $\text{Si} > 3$ apfu analyses, which are excluded by the models of Vidal et al. (2005) and
 Vidal et al. (2006), have the same $X\text{Fe}^{3+}$ ratio as the Si-poor analyses of the same sample.
 This assumption is supported by the consistency of the minimum $X\text{Fe}^{3+}$ values obtained for
 all the analyses ($\text{Si} < 3$ apfu) of any given sample. Even if these $X\text{Fe}^{3+}$ estimates are fraught
 with uncertainties, their input in the *T* calculations allows a sensitivity test of the various
 models with respect to $X\text{Fe}^{3+}$.

Regarding the illite case, we do not have a numerical method to estimate the Fe^{3+}
 content. However, the qualitative XANES study of Bourdelle (2011, *PhD*) showed that 2:1
 phyllosilicates of the Gulf Coast have a $\text{Fe}^{3+}/(\text{Fe}^{3+} + \text{Fe}^{2+})$ ratio higher than 50%. Because
 taking ferric iron into account implies an increase of calculated vacancies, the sensitivity of
 Dubacq et al. (2010) model to the $X\text{Fe}^{3+}$ had to be tested. This model was therefore applied to
 Gulf Coast illite under two limiting assumptions, with $X\text{Fe}^{3+} = 0$ (case 1) and $X\text{Fe}^{3+} = 0.7$
 (case 2).

349

350 **Results from Gulf Coast chlorites**

351 In order to test the available chlorite thermometers, we have selected for each present-
352 day P and T values only the three or four analyses that represent the closest approach to the
353 relevant equilibrium composition, referred to as “maximum zoning composition”. For the
354 empirical thermometers, these are the highest-^{IV}Al analyses; for thermodynamic models, these
355 are the extremum $\log K$ analyses (with > 80% overlap between the two sets), depending on
356 the direction of the reaction.

357 The application of all the *empirical* chlorite thermometers according to measured
358 temperature for the Gulf Coast samples shows that calculated T are systematically
359 overestimated with respect to measured T . The thermometers of Cathelineau (1988),
360 Kranidiotis and McLean (1987), Jowett (1991) and Xie et al. (1997) predict a maximum
361 temperature of 360 ± 20 °C for the measured temperature of 216 °C. These four different
362 chlorite thermometers give similar results, showing the weak impact of the XFe corrections in
363 the equations. Using the Zang and Fyfe (1995) equation, in which XFe has a stronger
364 influence on the temperature estimation, the calculated temperatures are closer to measured
365 temperatures, but still too high, e.g. 286 °C for a measured temperature of 216 °C. Hillier and
366 Velde (1991) equation gives the closest, but the most scattered, temperature estimates to
367 measured temperature, with results between 75 and 380 °C. Interestingly, their calibration is
368 the only one that includes Gulf Coast chlorites (for which they pointed out the high ^{IV}Al
369 content).

370 Temperature estimations obtained with the *thermodynamic* models of Walshe (1986),
371 Inoue et al. (2009) and Vidal et al. (2005, 2006) models are represented on Figure 4, with all
372 iron considered as Fe²⁺ (case 1) and with Fe³⁺ as obtained with the Vidal et al. (2005, 2006)
373 convergence method and assumed to replace ^{VI}Al (case 2).

374 In the case of $\text{Fe}_{\text{total}} = \text{Fe}^{2+}$, all the thermometers overestimate temperatures. The Walshe
375 (1986) thermometer gives a temperature trend between 205 °C and 323 °C for present-day
376 temperatures of 102 °C and 216 °C, respectively. Although the results obtained for samples at
377 204 °C and 232 °C are out of the general trend, this model overestimates systematically
378 temperatures by an average of ~70 °C — and excludes many Si-poor analyses ($\text{Si} < 3$ apfu)
379 due to inappropriate choice of end-members. The results obtained with the Inoue et al. (2009)
380 method show a systematic trend of T overestimation by ~40 °C on the low- T side to ~70 °C
381 on the high- T side (Fig. 4). The model of Vidal et al. (2005, 2006), which excludes many
382 analyses ($\text{Si} > 3$ apfu), gives more scattered results but these are in better agreement with
383 measured temperatures and distributed on either side of the 1:1 line, with an average deviation
384 between calculated temperatures and BHT of 7 °C, against 65 °C and 59 °C for Inoue et al.
385 (2009) and Walshe (1986) models, respectively.

386 Taking into account the Fe^{3+} content, all thermodynamic models give lower or less
387 dispersed temperatures (Fig. 4). Regarding the Vidal et al. (2005, 2006) model, the most
388 visible effect of the ferric iron is the narrowing of the data scatter. The calculated T values
389 decrease compared to the same dataset without Fe^{3+} content when they are higher than 150
390 °C, and increase when they are below 150 °C. These trends were also noticed by Inoue et al.
391 (2009) as they tested the effect of Fe^{3+} on the Vidal et al. (2001) model. Temperatures
392 calculated with the Walshe (1986) model are slightly but consistently lower when a minimum
393 Fe^{3+} content is considered, by about 15 °C on average. Maximum calculated temperatures
394 range from 190 °C to 308 °C for the present-day temperatures of 102 °C to 216 °C,
395 respectively. The Fe^{3+} content has a limited effect and the temperature overestimation
396 persists. In the same way, the results given by the thermometer of Inoue et al. (2009) are
397 systematically lower when Fe^{3+} content is considered, by about 20 °C on average, even if for a
398 few analyses the shift can be as large as 100 °C ($X\text{Fe}^{3+} = 0.3$). New temperatures remain

overestimated for most of them, for instance they spread between 140°C and 181°C for a measured T of 102 °C, between 134 °C and 285 °C for a measured T of 191 °C, and between 261 °C and 325 °C for a measured T of 216 °C.

Results from Gulf Coast K-deficient micas

As for chlorite, the available illite thermometers were tested using only the three or four analyses that may be the closest to the “maximum zoning composition” for each present-day P and T . For the empirical thermometers, these are the highest-K analyses; for thermodynamic models, these are the extremum $\log K$ analyses (with > 85% overlap between the two sets), depending on the direction of reaction.

The empirical illite thermometer (Battaglia, 2004) gives results that show a positive correlation with the measured temperatures (Fig. 5), but with a systematic shift by an average of about +40-50 °C at high T and about +60-70 °C at low T .

The thermodynamic model of Dubacq et al. (2010) yields for each analysis of illite in equilibrium with quartz a P - T - $m\text{H}_2\text{O}$ stability relation. In the present case, the measured pressure was used as input value to calculate the temperature and hydration state. The results obtained with $\text{Fe}_{\text{total}} = \text{Fe}^{2+}$ (Fig. 6) show that most calculated temperatures are slightly overestimated (by less than 50 °C) and are less well correlated with measured T than with the Battaglia (2004) thermometer. Maximum temperatures range from 165 °C to 256 °C for measured 121 °C and 216 °C respectively, and 230 °C for measured 232 °C. If the calculations are made assuming $X\text{Fe}^{3+} = 0.7$ on the basis of preliminary STXM-XANES data, the results show (Fig. 6) a very similar pattern of overestimation, but with a slightly wider data scattering than with pure Fe^{2+} .

Results from illite-chlorite assemblages

To use illite + chlorite thermometers, three or four illite-chlorite pairs of rim analyses, located at less than 50 nm on either side of the illite-chlorite interface, were retained for each sample, whenever possible. When testing the effect of ferric iron, we used the same input data as above, i.e. $X\text{Fe}^{3+}$ ratio varying between 0.1 and 0.45 in chlorite as obtained with the Vidal et al. (2005, 2006) method, and the fixed value of 0.7 in illite-like phases according to STXM-XANES results.

In the case of the Walshe (1986) method, $\log K$ is negatively correlated with temperature, and the selected pairs are those yielding the lowest $\log K$ values. The reaction involved in the Walshe (1986) calculation requires the presence of K-feldspar in the assemblage, which was observed by SEM in most of our samples. The resulting calculated temperatures show a positive correlation with the measured temperatures (Fig. 7), provided the 102 °C sample is considered as an outlier, but they are generally overestimated by ~0-60 °C. Results show a trend between 133-172 °C for a measured 121 °C to 272-320 °C for a measured 232 °C. The Fe^{3+} content has no effect as the corresponding temperatures differ from the previous ones by only 3 to 4 °C.

The results of the multi-equilibrium calculation based on Vidal et al. (2005, 2006) model and Dubacq et al. (2010) hydration model are shown in Figure 8. As consideration of Fe^{3+} was shown to hardly improve chlorite thermometry and to slightly affect illite thermometry with these database and solution models, only calculations with minimum $X\text{Fe}^{3+}$ are presented here. Unlike most other models, the calculated temperatures (calculation from BHP; Fig. 8-b) are not clearly overestimated, but are within ± 50 °C of the measured temperatures. In contrast, the calculated pressures (Fig. 8-c) are not reliable, as they sometimes exceed 5 kbar, for a maximum measured value of 1.2 kbar.

Discussion

The need for spatially highly resolved analyses and relevant analyses selection for clay thermometry

The fine-scale compositional variations of low-*T* chlorites and illites were studied on diagenetic crystals as a function of increasing *P-T* conditions with a very high spatial control on microtextural interactions. Using this protocol, the presence of an intra-crystalline chemical zonation in low-*T* crystals was clearly established. The composition of the grain rims seems to respond to the *P-T* variations and therefore to approach equilibrium while the crystal core may preserve relic compositions. However, the dispersion at each temperature of crystal-rim compositions, for both illite and chlorite, indicates that rim compositions do not all record the last, highest-temperature equilibrium conditions but that some of them were acquired during earlier stages of equilibration during burial. Thus, the selection of analyses becomes a crucial point when trying to estimate the formation temperature and thermometry is not straightforward because the composition of each part of a crystal may refer to one part of the *P-T*/burial history. Using EMP would lead to average the crystal core-rim compositions, and to a biased application of geothermobarometers. In this way, it is clear that the use of TEM, with high spatial resolution, is highly recommended.

Evaluation of clay minerals thermometry and Fe³⁺ effect

In the chlorite case, the empirical approaches based on the aluminum content (Cathelineau 1988; Kranidiotis and McLean 1987; Jowett 1991; Hillier and Velde 1991; Zang and Fyfe 1995; Xie et al. 1997) give disparate temperatures and overestimate the temperature of our Gulf Coast samples by up to 170°C with respect to BHT, taken as indicative of the maximum burial conditions insofar as the subsidence has been continuous since the Cretaceous. In contrast, the temperature estimated with the models of Vidal et al. (2005,

2006) and Inoue et al. (2009) [as well as the chlorite + mica + K-feldspar + quartz + water equilibrium of Walshe (1986)] are in fair agreement with the BHT. This difference in the results between empirical calibrations and thermodynamic approaches suggests that empirical chlorite thermometers are inaccurate, most likely because of their inability to account properly for bulk-rock compositional effects. This conclusion is in line with the results of earlier studies by De Caritat et al. (1993) and Essene and Peacor (1995), which concluded that the empirical thermometers based on the ^{IV}Al content of chlorite are inaccurate and should be used with caution. In this context, the use of a spatially highly resolved analytical approach cannot help to improve the results.

The temperatures estimated from chlorite compositions with the non-empirical thermodynamic approach of Vidal et al. (2005, 2006) are in better agreement with the BHT, but the calculated temperatures are slightly scattered. Moreover, the numerous chlorite analyses showing high Si content (> 3 apfu) cannot be handled with this model. The semi-empirical approaches proposed by Walshe (1986) and especially by Inoue (2009) yield temperature estimates higher than but still in reasonable agreement with the BHT. As in the case of Vidal et al. (2005, 2006) model, the Walshe (1986) formalism cannot handle all the chlorite compositions measured in our samples, and is limited to chlorite with $Si > 3$ pfu. Only the formalism of Inoue et al. (2009) can be used for the entire set of compositions measured for Gulf Coast samples.

The present study also shows the strong effect of the distinction between Fe^{3+} and Fe^{2+} (Fig. 4) and confirms previous observations (Vidal et al. 2006; Inoue et al. 2009). The consideration of Fe^{3+} content increases the number of octahedral vacancies and reduces the R^{2+} occupancy. As octahedral vacancy (sudaite content and activity) is negatively correlated with T , the reduced R^{2+} occupancy generally results in a lower calculated temperature. However, the temperature variation due to the introduction of Fe^{3+} content is different for

each thermometer. Inoue et al. (2009) model is the most sensitive to ferric iron (Fig. 4), with a T variation between cases 1 and 2 ranging from 7 to 108 °C, compared to 6-49 °C for Walshe (1986) model and 0-59 °C for Vidal et al. (2005; 2006) model (Fig. 4). The choice of a random-mixing repartition of cations in the model of Inoue et al. (2009) seems to be the reason for this difference, because the vacancy number has a greater weight in the $\log K$ calculation of random-mixing models than in the ordered model. Surprisingly, the Vidal et al. (2005, 2006) model is the only one for which Fe^{3+} consideration increases the calculated temperatures at low- T and decreases them at high- T . In summary, all the thermodynamic models give overestimated and scattered temperatures if all iron is assumed as ferrous; taking into account a minimum Fe^{3+} occupancy leads to reduce the overestimation, whereas the results still remain slightly scattered. The valence state of iron is therefore not the sole reason for the inaccuracy of chlorite thermodynamic thermometers.

The observed scatter of results can be due to some errors, which stem from the uncertainties in BHT, in the thermodynamic standard-state properties of the end-members and solution models, departure of the analysed compositions from equilibrium compositions, and analytical uncertainties. The source of error resulting from the uncertainties associated with the thermodynamic data is difficult to estimate, because the thermodynamic data used for example by Vidal et al. (2005, 2006) model were calibrated using experimental and natural data of various levels of confidence. However, it is likely that the uncertainties in the thermodynamic data have a systematic effect on the calculated locations of the chlorite+quartz equilibrium. Moreover, the uncertainties in the thermodynamic data cannot be put forward in the case of Inoue et al. (2009) model, which is semi-empirical and not based on thermodynamic properties.

Even if the thermodynamic data were perfect, imprecision in the analysed compositions of minerals places limits on the accuracy with which T can be known. The scatter resulting from

the variation of the chlorite compositions within specific bounds given by the precision of the TEM analysis (element-dependent) can be calculated with a Monte Carlo technique (Lieberman and Petrakakis 1991). Thus, the effect of analytical uncertainties was simulated (i) to confirm that the observed compositional variations are significant and not due to the inaccuracy of analyses and (ii) to compare the accuracy of each thermometer by the evaluation of the sensitivity of the equilibrium K constant calculation to a slight variation of composition. In this MonteCarlo study, we focussed on the chlorite models of Walshe (1986), Vidal et al. (2005, 2006) and Inoue et al. (2009) because they yield similar thermometric results and thus could be distinguished by their precision, i.e. their sensitivity to the error factors. Starting from three Gulf Coast chlorite compositions (at 129, 204 and 232 °C as example), a Gaussian error distribution with $1\sigma = 1\%$ relative for all oxides was randomly sampled around the nominal weight percentage for each oxide in chlorite. This deviation of 1% for each oxide from the nominal composition was assumed to represent the TEM analytical uncertainties (as Vidal and Parra, 2000); 250 permutations led to the simulation of 250 mineral compositions. The set of simulated chlorite compositions was used to calculate 250 separate temperatures (noted “simulated temperatures”); Fe^{3+} content was recalculated each time. The maximum permissible scatter from the ‘nominal’ temperature estimate (from nominal chlorite) was fixed to a 95% confidence level. Indeed, 238 of the 250 simulated temperatures represent the assumed maximum temperature scatter, and therefore the influence of analytical uncertainties on temperature calculation. Results are presented in Figure 9. The observed variations of chemical compositions (Fig. 2 and 3) and the resulting variations of temperature estimates are clearly one order of magnitude larger than the possible effect of analytical uncertainties. For the Walshe (1986) model, 95% of simulated temperatures are separated by less than 10.7, 12.1 and 12.8 °C from the three nominal temperature estimates (190, 185 and 184 °C), respectively (Fig. 9). For the Vidal et al. (2005, 2006) model, the

absolute deviation is slightly higher than for the Walshe (1986) model, with 95% of simulated temperatures separated by less than 19, 17.4 and 14.8 °C from nominal temperature estimates (132, 211, 203 °C), respectively (Fig. 9). Finally, a higher absolute deviation of simulated temperatures is obtained for the Inoue et al. (2009) model, with 95% of simulated temperatures separated by a maximum of 15.7, 26.8 and 26.0 °C from nominal temperature estimates (143, 234, 235 °C), respectively (Fig. 9). These results show that the thermometer of Inoue et al. (2009) is the most sensitive to compositional variations, involving a dependence between the accuracy of analyses and that of the temperature calculation. Therefore, the relative accuracy (noted RA; $RA = \text{absolute deviation represented by 95\% of simulated temperatures} \times 100 / \text{Estimated } T$) of the Inoue thermometer is consistently higher by more than 10.9%, whereas Vidal et al. (2005, 2006) model has a $RA < 8.2\%$ (excepted for BHT = 129 °C) and Walshe (1986) model has a $RA < 7\%$ (Fig. 9). Paradoxically, we observe that Walshe (1986) proposed a geothermometer with a very good reproducibility of estimates, but with a very rough accuracy. In fact, the best compromise between sensitivity to analytical uncertainties and accuracy of temperature is given by Vidal et al. (2005, 2006) model.

In the illite case, the empirical thermometer of Battaglia (2004) gives temperatures overestimated compared to the present-day temperatures. Remarks made against chlorite empirical thermometers are also valid in the illite case. Moreover, the equation correction involving $|\text{Fe-Mg}|$, as proposed by Battaglia (2004), has no crystal-chemical basis. The temperatures estimated with the model of Dubacq et al. (2010) show the same increasing trend as measured temperatures and are not excessively scattered, especially at “high”- T (> 180 °C). At lower temperature, the calculated temperatures may be overestimated by more than 50°C, but not systematically. This may be due to the difficulty to take into account purely potassic, charge-deficient 2:1 phyllosilicates at low- T . The addition of Fe^{3+} content

deteriorates the correlation, and the estimated temperatures are slightly increased and scattered, involving a recommendation for a pure- Fe^{2+} application as mentioned by the authors.

Concerning the illite-chlorite assemblage, the Walshe (1986) formalism for chlorite + mica + quartz + K-feldspar + water equilibrium yields calculated temperatures that are positively correlated with measured T (Fig. 7). For $\text{Fe}_{\text{total}} = \text{Fe}^{2+}$, this model allows one to obtain results with a better accuracy (50 °C on average) than those obtained with Walshe's chlorite + quartz thermometer, and the addition of Fe^{3+} content changed the calculated T by only ~4 °C. The 'multi-equilibrium' approach combining Vidal et al. (2006) model for chlorite and Dubacq et al. (2010) model for smectite-illite-phengite gives plausible temperatures (Fig. 8): all temperatures boxes overlap the shaded area of BHT \pm 50°C. However, several estimates yield too high temperatures, such as samples at 216 °C (BHT) for which the calculated T is overestimated, or one sample at 191 °C (BHT), for which the calculated T range is large (up to 339 °C). Nevertheless, the 'multi-equilibrium approach', combined to the fine-scale analytical protocol, gives satisfactory temperature estimates, showing the importance of analyses selection.

In summary, the two illite + chlorite models tested here give reliable results. In fact, the protocol enables to measure equilibrium compositions of both illite and chlorite at the nanoscale. These results suggest that it is likely the scale at which the heterogeneous equilibrium illite + chlorite is achieved. This allows for relating the different equilibrium compositions and gives a good basis for thermobarometry at low temperature.

Chlorite and illite barometry

The thermodynamic model of Vidal et al. (2005, 2006) is the only chlorite-based model to consider the pressure parameter. Applied to metamorphic rocks, it has shown the importance of pressure on the chemical composition variations (e.g. Malasoma and Marroni, 2007). However, in a low- P /low- T diagram, the equilibrium curves calculated from our chlorite analyses are almost parallel to the P axis, which means that the chemical variations in chlorite are essentially dependent on temperature, thus confirming the validity of the assumption of Inoue et al. (2009). The model of Dubacq et al. (2010) considers the pressure as a significant parameter for the case of illite. Unlike the chlorite + quartz equilibrium curve, the illite + quartz equilibrium curve is not parallel to the P axis, and is P - T -dependent. However, the dP/dT slope of this curve is steep, and for the P - T domain investigated in this study, the model of Dubacq et al. (2010) predicts a higher T -dependence than P -dependence for illite composition. Moreover, the pressure uncertainty is as large as the entire range of pressure variations in diagenesis, which precludes any reliable estimate. Similarly, the pressure conditions constrained by the chlorite + illite equilibrium remain uncertain (Fig. 8-c), because of the steep slope of the illite + quartz equilibrium curve: except for one sample at 1.05 kbar (BHP), all measured pressures are located in the calculated pressure ranges, but these ranges are large (up to 11 kbar). In fact, the pressure effect on the low- T phyllosilicates appears to be too low compared to the temperature impact in this realm, involving a relative failure of the barometers to give results with acceptable error deviation.

Concluding Remarks

The analytical protocol proposed by Bourdelle et al. (2012) makes it possible to obtain data at the nanometer scale and to distinguish crystal-rim and -core analyses, allowing one to analyse the illite-chlorite interfaces and the calculation of illite-chlorite equilibrium. In fact,

the difference of chemical composition between rims and cores may be very significant, in particular for the illite K content. Moreover, these chemical parameters generally show a T -dependence that is the base of many thermometers, making the consideration of chemical zonation a crucial point. In this respect, the present study showed the difference of impact and reliability for the two variables: temperature and pressure. The pressure does not affect the chlorite, but the illite composition. From the results of Vidal et al. (2005, 2006) and Dubacq et al. (2010) models, the chlorite + quartz equilibrium seems to be essentially T -dependent at low grade, whereas the illite + quartz equilibrium is influenced by both temperature and pressure. However, if the T estimate is realistic, the P prediction remains difficult and inaccurate.

Nevertheless, from a thermometric point of view, empirical and thermodynamic approaches lead to disparate results. The empirical chlorite thermometers all overestimate the temperature of the studied samples, because the T -dependent ^{IV}Al or K variation alone is not an exclusive quantitative relation, and the common correction, based on XFe, does not improve the situation. The results of thermodynamic models are generally much more realistic (e.g. Vidal et al. 2005, 2006; Inoue et al. 2009; Dubacq et al. 2010 [in particular for $T > 180$ °C], Walshe, 1986 [for the chlorite + mica + quartz + K-feldspar + water equilibrium], and multi-equilibrium illite + chlorite approach), but revealed the importance of taking into account the Fe^{3+} content, in particular in the case of chlorite disordered models.

The main difference between the semi-empirical or non-empirical thermodynamic and the empirical approaches is that the former are based on the ratio of chlorite end-members activities (equilibrium constant K). The same $\log K$, and therefore the same temperature estimate can be obtained for chlorites of different compositions. Such approaches are thus compatible with the observation that chlorites crystallizing at the same temperature in rocks of different bulk compositions have different compositions. In contrast, such observation

cannot be accounted for by the empirical thermometers based on the ^{IV}Al content, even corrected using the Mg and Fe content (e.g. Karnidiotis and McLean 1987). Moreover, thermodynamic models make illite + chlorite thermometry possible in the low- T domain. Therefore, the chlorite + mica + quartz + K-feldspar + water thermometer proposed by Walshe (1986) and the combination of Dubacq et al. (2010) and Vidal et al. (2005, 2006) models give satisfactory results on Gulf Coast phyllosilicates, suggesting local equilibrium between illite and chlorite along crystal rims. The prerequisite for such results is that thermodynamic models are combined with an analytical technique that can resolve the very fine-scale compositional readjustments or overgrowths that may witness an approach of local equilibrium and keep a record of it. However, the choice of end-members for thermodynamic models can become a limitation depending on the composition domain studied. Indeed, the models of Vidal et al. (2005, 2006) and Walshe (1986) have the drawback to exclude many chlorite analyses with Si content higher or less than 3 apfu, respectively, which is unfortunately a common case for low- T chlorites. Altogether, the thermodynamic approaches, based on the ratio of chlorite end-members activities, are compatible with the observation that chlorites crystallizing at the same temperature in rocks of different bulk compositions have different compositions. This study however stresses that recent models yield accurate results only if the compositional data used consider the chemical intracrystalline zonation occurring in low- T clay crystals. This requires the use of nanoscale chemical analysis.

Acknowledgements

672 We are most grateful to the materials characterization department of IFP Energies nouvelles-
673 Lyon, in particular to F. Moreau, and to the laboratory of CP2M-Université Aix-Marseille, for
674 technical advice. Thanks are also extended to K. Milliken, S. Dutton and J. Donnelly of
675 Bureau of Economic Geology at Austin. The discussions and comments of the journal editor
676 R. Yuretich and of P. Aagaard are gratefully acknowledged. This study was financially
677 supported by IFP Energies nouvelles, CNRS and ENS Paris.

678

679 **References**

680

681 Bailey, S.W. (1988) Chlorites: structures and crystal chemistry. In S.W. Bailey, Eds.,
682 Hydrous Phyllosilicates (Exclusive of Micas), p. 347-403. Mineralogical Society of America,
683 Washington D.C.

684 Battaglia, S. (2004) Variations in the chemical composition of illite from five geothermal
685 fields: a possible geothermometer. *Clay Minerals*, 39, 501-510.

686 Bebout, D.G., Weise, B.R., Gregory, A.R., and Edwards, M.B. (1982) Wilcox sandstone
687 reservoirs in the deep subsurface along the Texas Gulf Coast. 125 p. University of Texas,
688 Austin.

689 Bodner, D.P. (1985) Heat variations caused by groundwater flow in growth faults of the
690 South Texas, Gulf Coast basin, 187 p. Ph.D. thesis, University of Texas, Austin.

691 Bodner, D.P. and Sharp, J.M. (1988) Temperature variations in South Texas subsurface.
692 *American Association of Petroleum Geologists Bulletin*, 72, 21-32.

693 Bourdelle, F. (2011) Thermobarométrie des phyllosilicates dans les séries naturelles:
694 Conditions de la diagenèse et du métamorphisme de bas degré, 318 p. Ph.D. thesis, University
695 Paris-Sud, Orsay.

696 Bourdelle, F., Parra, T., Beyssac, O., Chopin, C., and Moreau, F. (2012) Ultrathin section
 697 preparation of phyllosilicates by Focused Ion Beam milling for quantitative analysis by TEM-
 698 EDX. *Applied Clay Science*, 59-60, 121-130.

699 Cathelineau, M. (1988) Cation site occupancy in chlorites and illites as a function of
 700 temperature. *Clay Minerals*, 23, 471-485.

701 Cathelineau, M. and Nieva, D. (1985) A chlorite solid solution geothermometer. The Los
 702 Azufres (Mexico) geothermal system. *Contributions to Mineralogy and Petrology*, 91, 235-
 703 244.

704 De Caritat, P., Hutcheon, I., and Walshe, J.L. (1993) Chlorite geothermometry: a review.
 705 *Clays and Clay Minerals*, 41, 219-239.

706 Dodge, M.M. and Posey, J.S. (1981) Structural cross sections, Tertiary formations, Texas
 707 Gulf Coast. University of Texas, Austin.

708 Dubacq, B., Vidal, O., and De Andrade, V. (2010) Dehydration of dioctahedral aluminous
 709 phyllosilicates: thermodynamic modelling and implications for thermobarometric estimates.
 710 *Contributions to Mineralogy and Petrology*, 159, 159-174.

711 Dutton, S.P. and Loucks, R.G. (2010) Diagenetic controls on evolution of porosity and
 712 permeability in lower Tertiary Wilcox sandstones from shallow to ultradeep (200-6700 m)
 713 burial, Gulf of Mexico Basin, USA. *Marine and Petroleum Geology*, 27, 69-81.

714 Essene, E.J. and Peacor, D.R. (1995) Clay mineral thermometry - A critical perspective. *Clays*
 715 *and Clay Minerals*, 43, 540-553.

716 Heaney, P.J., Vicenzi, E.P., Giannuzzi, L.A., and Livi, K.J.T. (2001) Focused ion beam
 717 milling: A method of site-specific sample extraction for microanalysis of Earth and planetary
 718 materials. *American Mineralogist*, 86, 1094-1099.

719 Helgeson, H.C., Delany, J.M., Nessbitt, H.W., and Bird, D.K. (1978) Summary and critique
 720 of the thermodynamic properties of rock-forming minerals. *American Journal of Science*,
 721 278A, 1-229.

722 Helgeson, H.C and Aagaard, P. (1985) Activity/composition relations among silicates and
 723 aqueous solutions. I. Thermodynamics of intrasite mixing and substitutional order/disorder in
 724 minerals. *American Journal of Science*, 285, 769-844.

725 Hillier, S. and Velde, B. (1991) Octahedral Occupancy and the Chemical-Composition of
 726 Diagenetic (Low-Temperature) Chlorites. *Clay Minerals*, 26, 149-168.

727 Holland, T.J.B., Baker, J., and Powell, R. (1998) Mixing properties and activity composition
 728 relationships of chlorites in the system $\text{MgO-FeO-Al}_2\text{O}_3\text{-SiO}_2\text{-H}_2\text{O}$. *European Journal of*
 729 *Mineralogy*, 10, 395-406.

730 Hutcheon, I. (1990) Clay carbonate reactions in the Venture area, Scotian Shelf, Nova Scotia,
 731 Canada. The Geochemical society, Special Publication, 2, 199-212.

732 Inoue, A., Meunier, A., Patrier-Mas, P., Rigault, C., Beaufort, D., and Vieillard, P. (2009)
 733 Application of Chemical Geothermometry to Low-Temperature Trioctahedral Chlorites.
 734 *Clays and Clay Minerals*, 57, 371-382.

735 Jahren, J.S. (1991) Evidence of Ostwald ripening related recrystallization of chlorites from
 736 reservoir rocks offshore Norway. *Clay Minerals*, 26, 169-178.

737 Jahren, J.S. and Aagaard, P. (1989) Compositional variations in diagenetic chlorites and
 738 illites, and relationships with formation-water chemistry. *Clay Minerals*, 24, 157-170.

739 Jahren, J.S. and Aagaard, P. (1992) Diagenetic Illite-Chlorite Assemblages in Arenites .1.
 740 Chemical Evolution. *Clays and Clay Minerals*, 40, 540-546.

741 Jiang, W.T., Peacor, D.R., and Buseck, P.R. (1994) Chlorite Geothermometry -
 742 Contamination and Apparent Octahedral Vacancies. *Clays and Clay Minerals*, 42, 593-605.

743 Jones, P.H. (1975) Geothermal and hydrocarbon regimes, Northern Gulf of Mexico basin. In
 744 M.H. Dorfman and R.W. Deller, Eds., Proceedings of the first geopressed geothermal
 745 energy conference, p. 15-89. University of Texas, Center for energy studies, Austin.

746 Jowett, E.C. (1991) Fitting iron and magnesium into the hydrothermal chlorite
 747 geothermometer. GAC/MAC/SEG Joint annual meeting, Toronto, Canada.

748 Kehle, R.O. (1971) Geothermal survey of North America. Annual progress report, American
 749 Association of Petroleum Geologists, 31 p.

750 Kohler, E., Parra, T., and Vidal, O. (2009) Clayey Cap-Rock Behavior in H₂O-CO₂ Media at
 751 Low Pressure and Temperature Conditions: An Experimental Approach. Clays and Clay
 752 Minerals, 57, 616-637.

753 Kisters, E.C., Bebout, D.G., Seni, S.J., Garrett, C.M., Brown, L.F., Hamlin, H.S., Dutton,
 754 S.P., Ruppel, S.C., Finley, R.J., and Tyler, N. (1989) Atlas of major Texas gas reservoirs. 168
 755 p. University of Texas, Austin.

756 Kranidiotis, P. and McLean, W.H. (1987) Systematics of chlorite alternation at the Phelps
 757 Dodge massive sulfide deposit, Matagami, Quebec. Economic Geology, 82, 1898-1911.

758 Lanson, B. and Besson, G. (1992) Characterization of the End of Smectite-to-Illite
 759 Transformation - Decomposition of X-Ray-Patterns. Clays and Clay Minerals, 40, 40-52.

760 Lieberman, J. and Petrakakis, K. (1991) TWEEQU Thermobarometry: Analysis of
 761 uncertainties and application to granulites from western Alaska and Austria. Canadian
 762 Mineralogist, 29, 857-887.

763 Loucks, R.G., Dodge, M.M., and Galloway, W.E. (1979) Sandstone consolidation analysis to
 764 delineate areas of high-quality reservoirs suitable for production of geopressed geothermal
 765 energy along the Texas Gulf Coast. 97 p. U.S. Department of energy, Austin.

766 Lynch, F.L. (1994) The effects of depositional environment and formation water chemistry on
 767 the diagenesis of Frio formation (Oligocene) sandstones and shales, Aransas, Nueces and San
 768 Patricio counties, Texas, 303 p. Ph.D. thesis, University of Texas, Austin.

769 Malasoma, A. and Marroni, M. (2007) HP/LT metamorphism in the Volparone Breccia
 770 (Northern Corsica, France): evidence for involvement of the Europe/Corsica continental
 771 margin in the Alpine subduction zone. *Journal of Metamorphic Geology*, 25, 529-545.

772 Mathieu, Y. and Velde, B. (1989) Identification of thermal anomalies using clay mineral
 773 composition. *Clay Minerals*, 24, 591-602.

774 McKenna, T.E. (1997) Geologic and hydrologic constraints on fluid and heat flow in
 775 overpressured rocks of the Rio Grande embayment, Gulf of Mexico basin, 241 p. Ph.D.
 776 thesis, University of Texas, Austin.

777 Nunn, J.A. (1984) Subsidence and temperature histories for Jurassic sediments in the
 778 Northern Gulf Coast: A thermal mechanical model. In D.G. Bebout, W.P.S. Ventress, B.F.
 779 Perkins and C.H. Moore, Eds., *The Jurassic of the Gulf rim*, p. 309-322. GCSSEPM
 780 Foundation 3th Annual Research Conference Proceedings, Houston, Texas.

781 Parra, T. (2001) Les équilibres chlorite-phengite : de l'étude de la lame mince aux calculs des
 782 trajets pression-température, 391 p. Ph.D thesis, Université Paris-Sud XI, Orsay.

783 Parra, T., Vidal, O., and Agard, P. (2002) A thermodynamic model for Fe-Mg dioctahedral K
 784 white micas using data from phase-equilibrium experiments and natural pelitic assemblages.
 785 *Contributions to Mineralogy and Petrology*, 143, 706-732.

786 Perry, E.A. and Hower, J. (1970) Burial diagenesis in Gulf Coast pelitic sediments. *Clays and*
 787 *Clay Minerals*, 18, 165-177.

788 Pfeiffer, D.S. (1989) Temperature variations and their relation to groundwater flow, South
 789 Texas, Gulf Coast basin, 198 p. Ph.D. thesis, University of Texas, Austin.

790 Posey, J.S. (1986) The Louann Salt of the Gulf Coast basin, with emphasis on South Texas. In
 791 W.L. Stapp, Eds., Contributions to the geology of South Texas, p. 440-446. South Texas
 792 Geological Society, San Antonio.

793 Royden, L., Sclater, J.G., and Von Her, R.P. (1980) Continental margin subsidence and heat
 794 flow: important parameters in formation of petroleum hydrocarbons. American Association of
 795 Petroleum Geologists Bulletin, 64, 173-187.

796 Shau, Y.H., Peacor, D.R., and Essene, E.J. (1990) Corrensite and mixed-layer
 797 chlorite/corrensite in metabasalt from northern Tawain: TEM/AEM, EMPA, XRD and optical
 798 studies. Contributions to Mineralogy and Petrology, 105, 123-142.

799 Stanley, S.M. (1986) Earth and life through time, 689 p. New York.

800 Trotet, F., Vidal, O., and Jolivet, L. (2001) Exhumation of Syros and Sifnos metamorphic
 801 rocks (Cyclades, Greece): new constraints on the P-T paths. European Journal of Mineralogy,
 802 13, 901-920.

803 Van Cappellen, E. and Doukhan, J.C. (1994) Quantitative Transmission-X-Ray Microanalysis
 804 of Ionic Compounds. Ultramicroscopy, 53, 343-349.

805 Velde, B. and Medhioub, M. (1988) Approach to chemical equilibrium in diagenetic chlorites.
 806 Contributions to Mineralogy and Petrology, 98, 122-127.

807 Vidal, O., De Andrade, V., Lewin, E., Munoz, M., Parra, T., and Pascarelli, S. (2006) P-T-
 808 deformation- $\text{Fe}^{3+}/\text{Fe}^{2+}$ mapping at the thin section scale and comparison with XANES
 809 mapping: application to a garnet-bearing metapelite from the Sambagawa metamorphic belt
 810 (Japan). Journal of Metamorphic Geology, 24, 669-683.

811 Vidal, O., Goffe, B., Bousquet, R., and Parra, T. (1999) Calibration and testing of an
 812 empirical chloritoid-chlorite Mg-Fe exchange thermometer and thermodynamic data for
 813 daphnite. Journal of Metamorphic Geology, 17, 25-39.

- Vidal, O. and Parra, T. (2000) Exhumation paths of high-pressure metapelites obtained from local equilibria for chlorite-phengite assemblages. *Geological Journal*, 35, 139-161.
- Vidal, O., Parra, T., and Trotet, F. (2001) A thermodynamic model for Fe-Mg aluminous chlorite using data from phase equilibrium experiments and natural pelitic assemblages in the 100 ° to 600 °C, 1 to 25 kb range. *American Journal of Science*, 301, 557-592.
- Vidal, O., Parra, T., and Vieillard, P. (2005) Thermodynamic properties of the Tschermak solid solution in Fe-chlorite: Application to natural examples and possible role of oxidation. *American Mineralogist*, 90, 347-358.
- Walshe, J.L. (1986) A six-component chlorite solid solution model and the conditions of chlorite formation in hydrothermal and geothermal systems. *Economic Geology*, 81, 681-703.
- Wirth, R. (2004) Focused Ion Beam (FIB): A novel technology for advanced application of micro- and nanoanalysis in geosciences and applied mineralogy. *European Journal of Mineralogy*, 16, 863-876.
- Xie, X.G., Byerly, G.R., and Ferrell, R.E. (1997) Iib trioctahedral chlorite from the Barberton greenstone belt: Crystal structure and rock composition constraints with implications to geothermometry. *Contributions to Mineralogy and Petrology*, 126, 275-291.
- Zang, W. and Fyfe, W.S. (1995) Chloritization of the Hydrothermally Altered Bedrock at the Igarape-Bahia Gold Deposit, Carajas, Brazil. *Mineralium Deposita*, 30, 30-38.

Figures

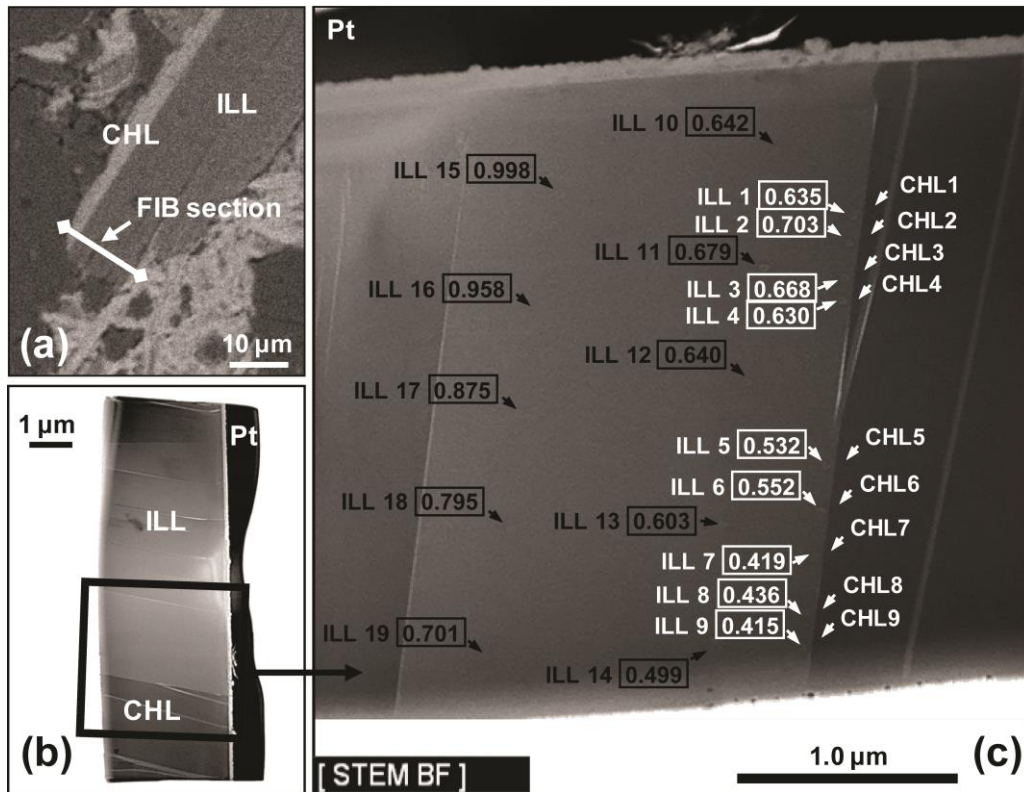


Figure 1: Analysis of an illite-like - chlorite assemblage, sample of Alamo#1 well, 5825 m. (a) SEM image of the petrographic thin section showing the emplacement of the FIB foil to be cut across the illite-like - chlorite interface. (b) Brigh-field TEM image of the FIB foil extracted from the section, with the platinum strap on top of it. (c) Enlargement with exaggerated image contrast in order to show the analysis points. Note their size as compared to scale bar, and their distribution. Analyses 1 to 9 are considered as rim analyses [white text], all others as core analyses [black text]. K contents are indicated for illite-like phase in apfu [in boxes]. Note the K content variation between crystal core and crystal rim.

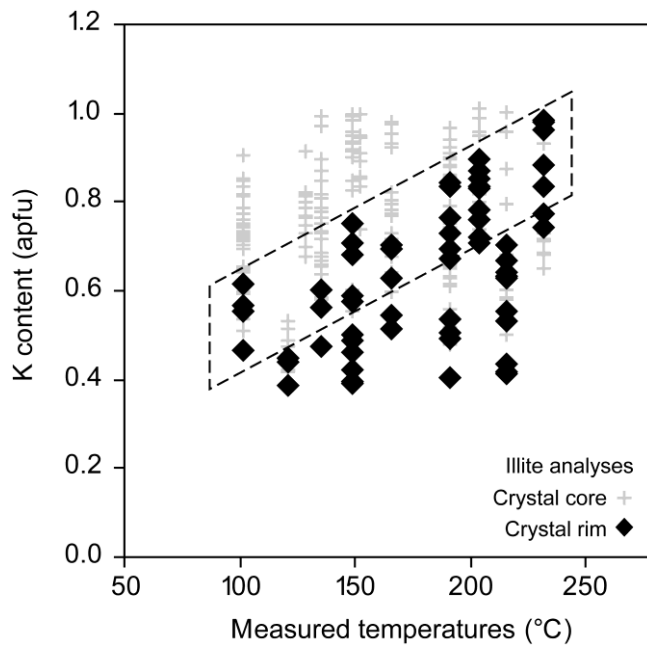
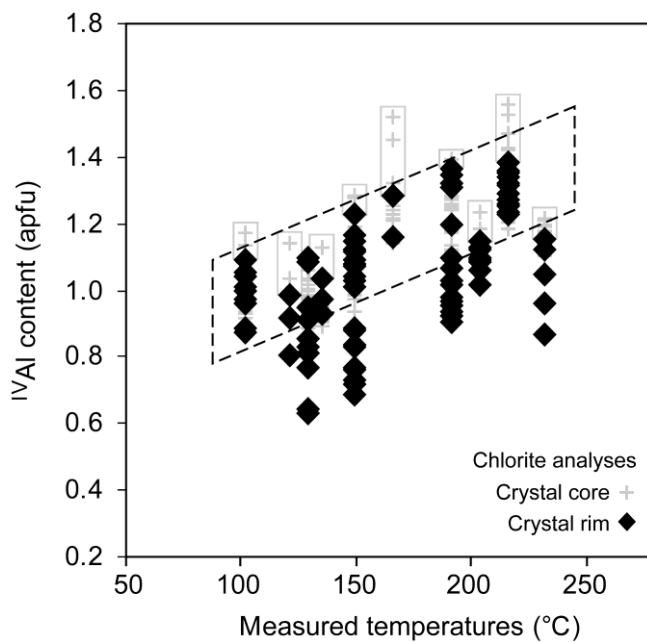


Figure 2: K contents of 2:1 phyllosilicates of Gulf Coast *versus* measured temperatures (corrected bottom-hole temperature, BHT). Comparison of crystal-rim and crystal-core analyses. The outlined area enclosed within dashed bands qualitatively underlines the trend drawn approximately by the “maximum illitization”, i.e. rims analyses which were assumed to represent the closest approach to relevant equilibrium composition.



853 Figure 3: ^{IV}Al contents of Gulf Coast chlorites *versus* measured temperatures (corrected
854 BHT). Comparison of crystal-rim and crystal-core analyses. The outlined area enclosed
855 within dashed band, qualitatively underlines the trend drawn approximately by the maximum
856 ^{IV}Al content in crystal-rims, which is assumed to represent the closest approach to relevant
857 equilibrium composition. Rectangles represent the difference between the maximum ^{IV}Al
858 content in rims and cores of chlorite grains.

859

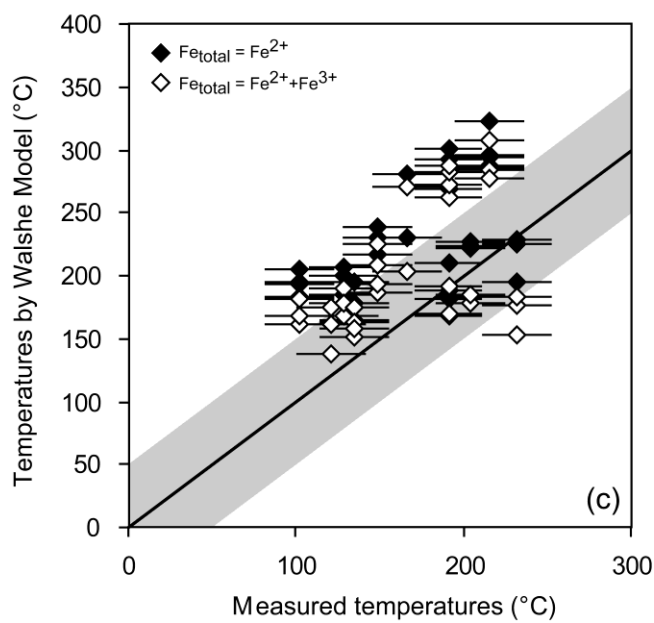
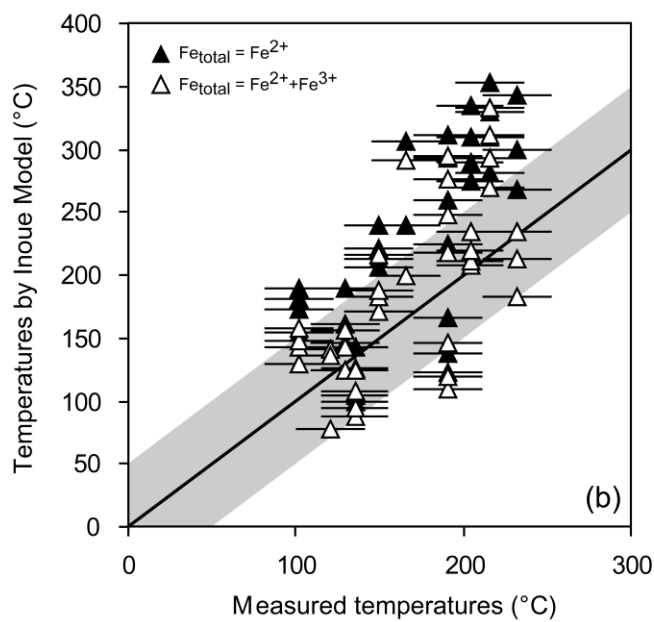
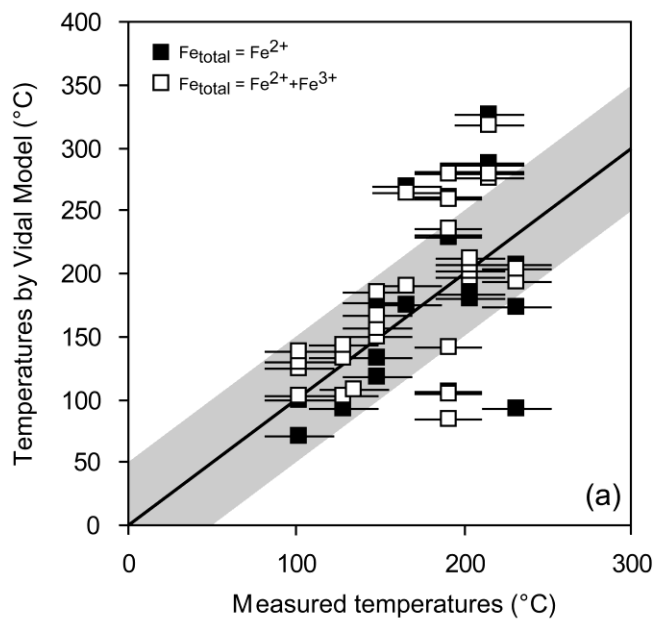


Figure 4: Comparison between measured temperatures (corrected BHT with an assumed error of 20 °C) and temperatures calculated with (a) Vidal et al. (2005, 2006) model, (b) Inoue et al. (2009) model and (c) Walshe (1986) model. Solid symbols, $\text{Fe}_{\text{total}} = \text{Fe}^{2+}$; open symbols, Fe^{3+} is considered (see text).

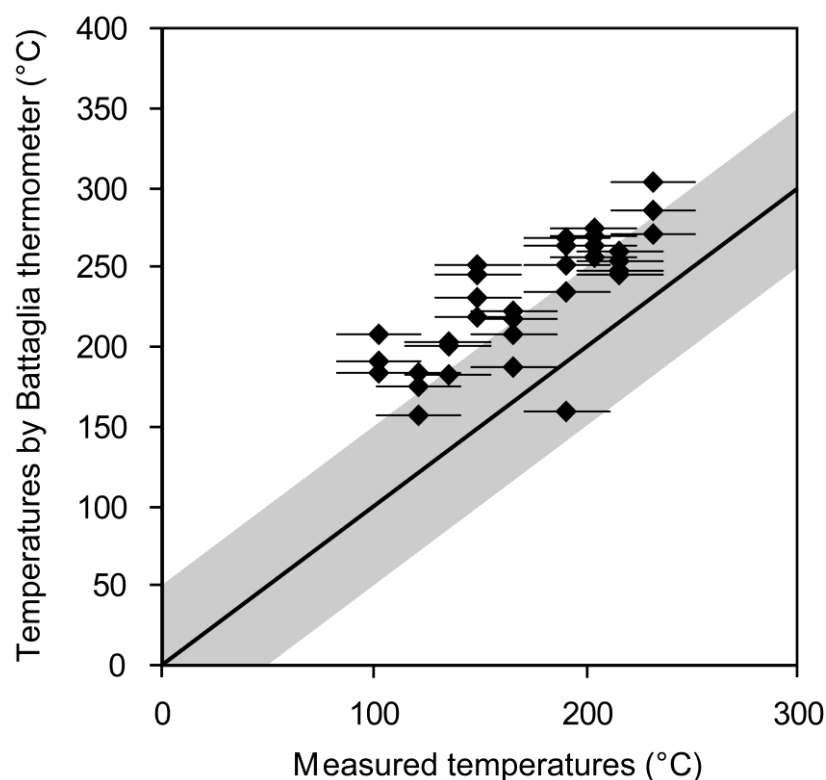


Figure 5: Comparison between measured temperatures (corrected BHT) and temperatures calculated with the empirical equation of Battaglia (2004). All Fe is considered as Fe^{2+} . Corrected BHT are represented with an assumed uncertainty of 20 °C.

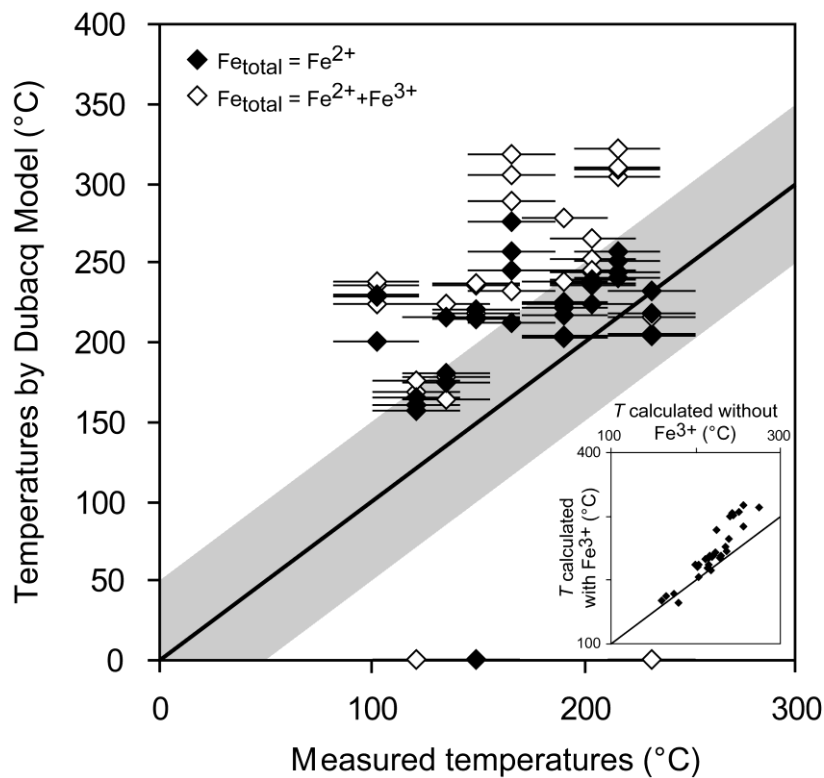
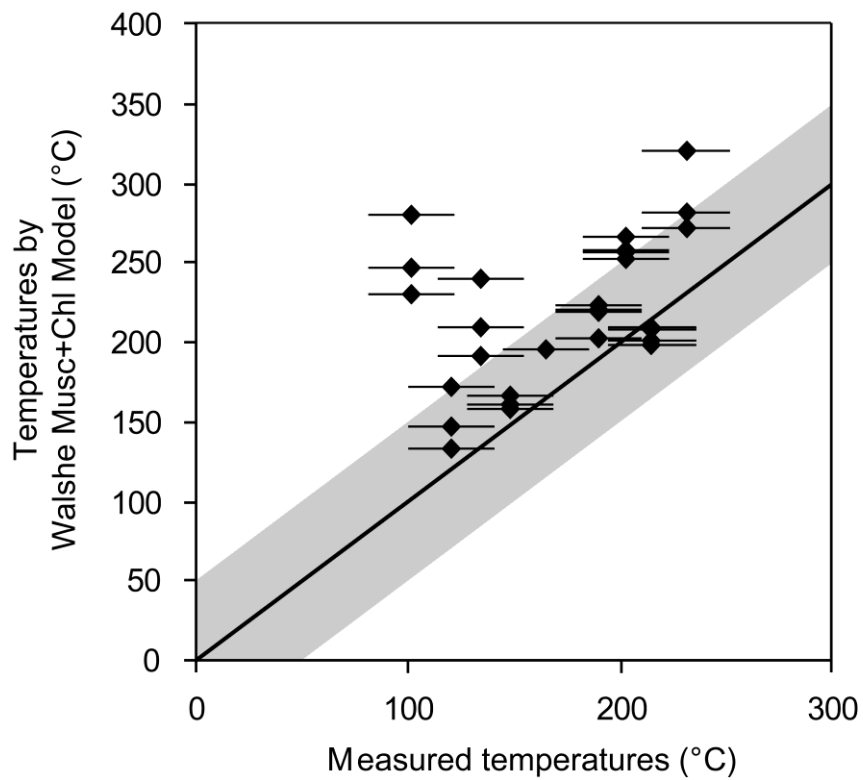


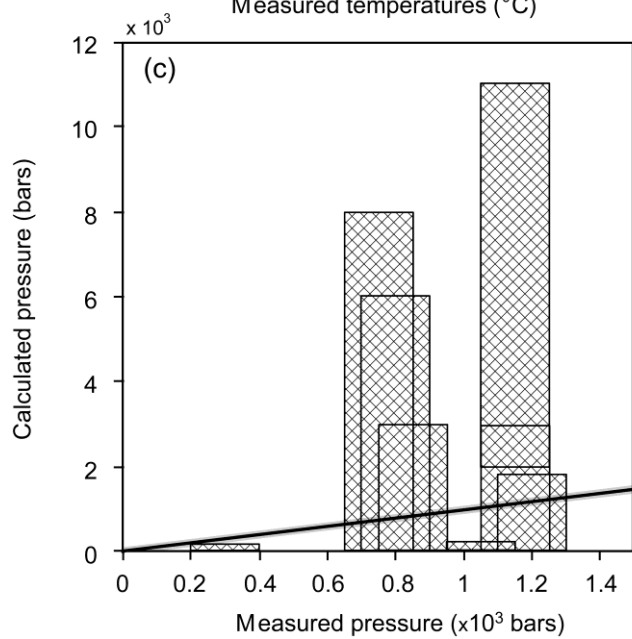
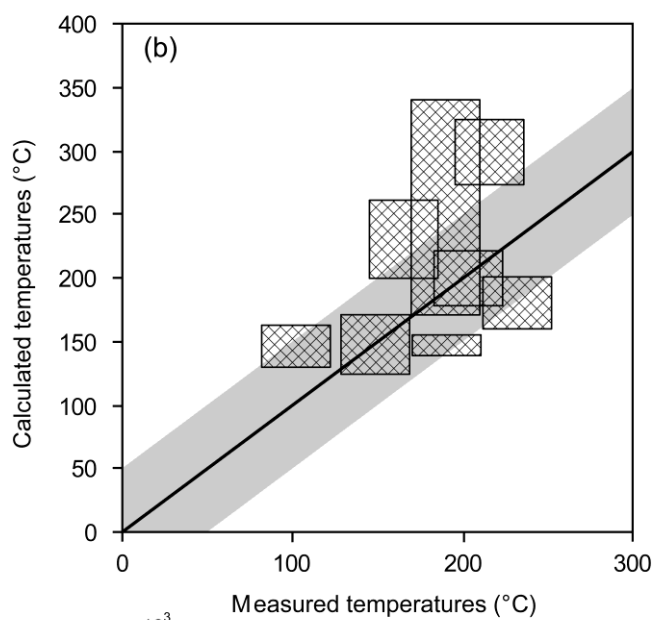
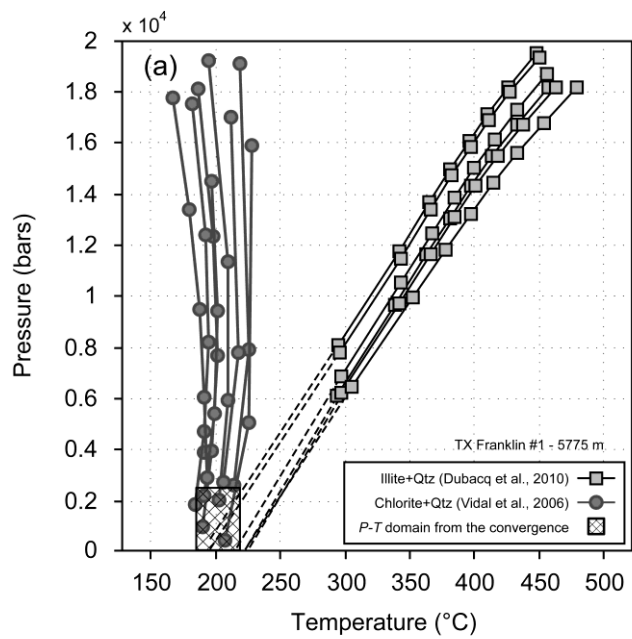
Figure 6: Comparison between measured temperatures (corrected BHT) and temperatures calculated with the thermodynamic model of Dubacq et al. (2010). Solid symbols: $\text{Fe}_{\text{total}} = \text{Fe}^{2+}$; open symbols: Fe^{3+} content is considered (see text). Corrected BHT are represented with an assumed uncertainty of 20 °C.



877

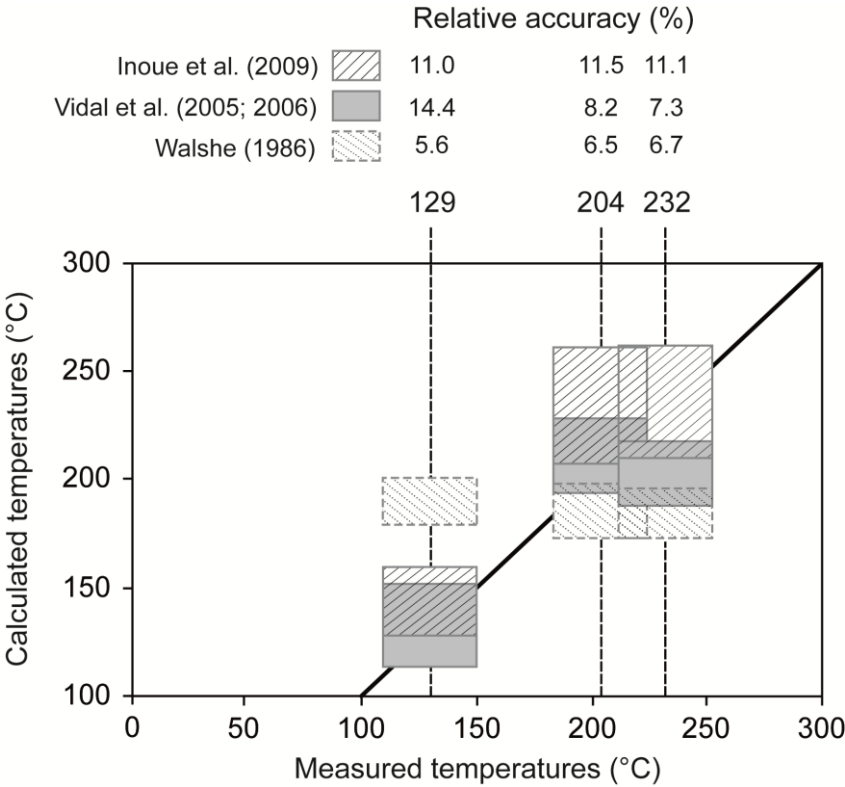
878 Figure 7: Comparison between measured temperatures (corrected BHT) and temperatures
 879 calculated with the model of Walshe (1986) for the equilibrium chlorite + illite + K-feldspar +
 880 quartz + water. All Fe is considered as Fe^{2+} . Corrected BHT are represented with an assumed
 881 uncertainty of 20 °C.

882



884 Figure 8: Temperatures and pressures obtained from the combination of the non-ideal ordered
 885 models of Vidal et al. (2005, 2006) and Dubacq et al. (2010) for Gulf Coast chlorites. (a)
 886 Example of equilibrium convergence for several chlorite and illite analyses of one Gulf coast
 887 FIB section. The square area represents the P - T domain of convergence. All chl-ill analysis
 888 pairs are used. (b) Calculated temperatures compared to measured temperatures. Square areas
 889 correspond to [in abscissa] the assumed uncertainty of 20 °C in BHT data, [in ordinate] the
 890 maximum and the minimum temperatures obtained from the convergence domain (defined
 891 from all chl-ill analysis pairs of all FIB sections for each P - T data). (c) Calculated pressures
 892 compared to measured pressures. Square areas correspond to [in abscissa] the assumed
 893 uncertainty of ± 100 bars in BHP data, [in ordinate] the maximum and the minimum pressures
 894 obtained from the convergence domain (defined from all chl-ill analysis pairs of all FIB
 895 sections for each P - T data).

896



897

Figure 9: Results in terms of temperature of the Monte-Carlo simulation for the three studied chlorite thermometers (Walshe, 1986; Inoue et al., 2009; Vidal et al., 2005 2006), for three nominal chlorites (at BHT = 129, 204 and 232 °C). The areas represent the assumed uncertainty of ± 20 °C on BHT in abscissa and the absolute accuracy obtained from a Monte-Carlo randomization on 250 chlorite compositions, with a 95% confidence level, in ordinate. Relative accuracy corresponds to absolute deviation x 100 / Estimated T .

Tables

Table 1: Selection of TEM-EDX analyses of Gulf Coast K-deficient mica: crystal rim analyses with the highest K content for each P - T . Atomic contents are given in atoms per formula unit (O = 11 apfu), and M1, M2 and M3 represent the cationic sites as defined by Dubacq et al. (2010). All iron is considered as ferrous. The analytical uncertainties are difficult to estimate, but are probably ± 1 -2 wt% for major elements and ± 1 -5 wt% for minor elements (Bourdelle *et al.*, 2012); the impact of an uncertainty of ± 1 wt% (for each element) on the thermometric estimations is discussed in the text.

Samples	AZ#159 9230	ST#470 10717	CK#2 12196	LA#1 13559	ST#356 14501	CW#1 14277	WR#C1 17805	FR#1 18946	AL#1 19110	AL#1 20711
Analysis	m42	m24	m24	m30	m13	m2	m33	m3	m34	M30
BHT (°C)	102	121	135	149	166	191	191	204	216	232
BHP (bars)	300	590	690	850	800	750	1050	1150	1150	1200
Si	3.38	3.78	3.44	3.41	3.10	3.43	3.37	3.30	3.18	3.32
Ti	0.01	0.01	0.01	0.02	0.02	0.00	0.03	0.02	0.00	0.02
^{IV} Al	0.62	0.21	0.55	0.58	0.89	0.57	0.59	0.68	0.82	0.66
^{VI} Al	1.87	1.53	1.82	1.75	1.86	1.90	1.48	1.57	1.74	1.59
Σ Al	2.48	1.74	2.37	2.32	2.75	2.46	2.07	2.25	2.56	2.25
Σ Fe ²⁺	0.07	0.20	0.10	0.11	0.16	0.14	0.35	0.26	0.30	0.23
Σ Mg	0.11	0.32	0.14	0.18	0.14	0.06	0.31	0.27	0.15	0.20
Mg (M1)	0.03	0.03	0.03	0.02	0.08	0.03	0.06	0.05	0.06	0.01
Fe ²⁺ (M1)	0.02	0.02	0.02	0.01	0.08	0.06	0.07	0.05	0.12	0.01
□(M1)	0.95	0.96	0.95	0.96	0.84	0.91	0.87	0.90	0.82	0.97
Mg (M2+M3)	0.08	0.29	0.10	0.16	0.07	0.03	0.24	0.22	0.08	0.19

Fe ²⁺ (M2+M3)	0.05	0.18	0.08	0.10	0.07	0.07	0.28	0.21	0.17	0.22
K	0.62	0.45	0.60	0.75	0.70	0.40	0.84	0.90	0.70	0.99
Na	0.04	0.03	0.03	0.00	0.00	0.05	0.00	0.00	0.00	0.03
Ca	0.00	0.06	0.00	0.00	0.00	0.02	0.00	0.00	0.00	0.00
v	0.35	0.46	0.37	0.25	0.30	0.53	0.16	0.10	0.30	0.00

Table 2: Selection of TEM-EDX analyses of Gulf Coast chlorites: crystal rim analyses with the highest ^{IV}Al content for each *P-T*. Atomic contents are given in atoms per formula unit (O=14 apfu), and M1, M2, M3 and M4 represent the cationic sites as defined by Vidal et al. (2005, 2006). All iron is considered as ferrous, value in bold indicates an analysis excluded by Vidal's model (Si > 3 apfu). The analytical uncertainties are difficult to estimate, but are probably ± 1 -2 wt% for major elements and ± 1 -5 wt% for minor elements (Bourdelle *et al.*, 2012); the impact of an uncertainty of ± 1 wt% (for each element) on the thermometric estimations is discussed in the text.

Sample	AZ#159 9230	ST#470 10717	CK#2 11924	CK#2 12196	LA#1 13559	ST#356 14501	CW#1 14277	WR#C1 17805	FR#1 18946	AL#1 19110	AL#1 20711
Analysis	chl28	chl30	chl50	chl20	chl23	chl34	chl31	chl16	chl29	chl25	chl29
BHT (°C)	102	121	129	135	149	166	191	191	204	216	232
BHP (bars)	300	590	660	690	850	800	750	1050	1150	1150	1200
Si	2.91	3.01	2.90	2.96	2.88	2.71	2.63	2.90	2.84	2.61	2.85
Ti	0.00	0.01	0.01	0.00	0.00	0.00	0.01	0.00	0.01	0.00	0.00
^{IV} Al	1.09	0.98	1.09	1.03	1.12	1.28	1.37	1.10	1.15	1.38	1.15
^{VI} Al	1.77	1.79	1.89	1.82	1.79	1.71	1.84	1.85	1.50	1.78	1.48
Σ Al	2.86	2.77	2.98	2.85	2.91	3.00	3.21	2.95	2.64	3.16	2.64
Σ Fe ²⁺	2.46	2.53	2.37	2.45	3.28	2.07	3.01	2.48	2.15	2.44	2.93
Σ Mg	1.39	1.22	1.31	1.34	0.53	1.98	0.85	1.28	2.11	1.55	1.36
Mg (M1)	0.22	-	0.19	0.20	0.08	0.26	0.09	0.18	0.36	0.17	0.23
Fe ²⁺ (M1)	0.39	-	0.35	0.37	0.52	0.27	0.32	0.36	0.37	0.27	0.51
Al (M1)	0.09	-	0.09	0.03	0.12	0.28	0.37	0.10	0.15	0.38	0.15
□(M1)	0.29	-	0.37	0.39	0.27	0.19	0.22	0.36	0.12	0.17	0.11
Mg (M2+M3)	1.17	-	1.12	1.14	0.44	1.72	0.76	1.09	1.75	1.38	1.12
Fe ²⁺ (M2+M3)	2.07	-	2.03	2.08	2.76	1.80	2.69	2.12	1.78	2.17	2.43
Al (M2+M3)	0.67	-	0.79	0.78	0.66	0.43	0.48	0.75	0.35	0.40	0.33
Al (M4)	1.00	-	1.00	1.00	1.00	1.00	1.00	1.00	1.00	1.00	1.00
XFe ³⁺	0.28	0	0.23	0.28	0.20	0.05	0.05	0.22	0.36	0.05	0.27

Table 3: Clay thermometry models tested in this study.

Model	Type	Variables	Assumptions	Other components
<i>Chlorite models</i>				
Cathelineau and Nieva (1985)	Empirical	T	^{IV}Al increase with T	
Walshe (1986) (1)	Thermodynamic	T	Chl+qz equilibrium	Random cation mixing
Kranidiotis and McLean (1987)	Empirical	T	^{IV}Al increase with T	Correction of bulk composition effect from Fe/(Fe+Mg)
Cathelineau (1988)	Empirical	T	^{IV}Al increase with T	
Jowett (1991)	Empirical	T	^{IV}Al increase with T	Correction of bulk composition effect from Fe/(Fe+Mg)
Hillier and Velde (1991)	Empirical	T	^{IV}Al increase with T	
Zang and Fyfe (1995)	Empirical	T	^{IV}Al increase with T	Correction of bulk composition effect from Fe/(Fe+Mg)
Xie et al. (1997)	Empirical	T	^{IV}Al increase with T	Correction of bulk composition effect from Fe/(Fe+Mg)
Vidal et al. (2006)	Thermodynamic	T - P	Chl+qz including non-ideality	Ordered cation mixing
Inoue et al. (2009)	Thermodynamic	T	Chl+qz	Random cation mixing Semi-empirical equation
<i>Illite/mica-like models</i>				
Battaglia (2004)	Empirical	T	K increase with T	Correction of bulk composition effect from Fe-Mg
Dubacq et al. (2010)	Thermodynamic	T - P hydration	Mica-like+qz including non-ideality	Ordered cation mixing
<i>Illite+chlorite models</i>				
Walshe (1986) (2)	Thermodynamic	T	Chl+mica+qz+feldspar	Random cation mixing
Vidal et al. (2006) + Dubacq et al. (2010)	Thermodynamic	T - P	Multi-equilibrium	Ordered cation mixing